

Numerical Study on Natural and Forced Convection in Electrochemical Cells

I.M. Sakr*, W.A. El-Askary, A. Balabel, K. Ibrahim

Mechanical Power Engineering Department, Faculty of Engineering
Menoufia University, Shebin El-Kom-EGYPT

Received: 19/05/2013 – Revised 21/06/2013 – Accepted 07/10/2013

Abstract

A numerically study has been performed to predict the dynamics of flow and mass transfer in the chemical solution of reactor. The solution exists between electrochemical cells. The mass and momentum conservation equations are used to describe the fluid motion. The code describes the effects of convection, diffusion, migration, chemical reaction and electrode reaction on the concentration, potential and current density distribution in an electrochemical reactor. The code has been tested through different cases including the prediction of flow in a binary electrolyte solution in natural convection and multi-ion electrochemical reactor where concentration, potential, current density distribution and concentration boundary layer can be compared with available experimental data and published numerical results.

Keywords: Natural/ forced convection; Multi-ion; Finite volume method; Turbulent Mass transfer; Current density distribution

1. Introduction

There exist many electrochemical systems in our daily lives, such as the metal electroplating, primary and secondary batteries, copper wiring technique in the microprocessor and graphic chip and the electrochemical pattern etching in electronic circuit design. Electrochemical cells appear in several industrial applications, such as copper refining cells and lead-acid batteries. Natural convection induced by variations of ionic concentration plays an essential role in electrochemical cells. It turns out that between the different transport mechanisms, convection, migration and convection controls in most applications. The fact that the liquid moves due to buoyancy influences the mass transport process considerably. The efficiency of the transport mechanisms in turn directly influences the process of interest in the cell. Hydrodynamics of electrochemical cells have been subject to many scientific and industrial investigations in the past few years. In general, ionic mass transfer is based on three different transport mechanisms, as outlined in Newman and Thomas-Alyea [1]: ionic mass transport as a result of a velocity field (convection), mass transfer as a result of concentration gradients (diffusion), and mass transfer as a result of an electric field (migration). In electrochemical cells, local density variations are caused by local variations of the ionic concentration. Such concentration gradients occur especially near electrode surfaces, where electrochemical reactions take place. In the case of a weak influence of forced convection, natural convection can have significant effects on the reaction rates along the electrodes or on the limiting currents. The influence of natural convection in electrochemical cells was already considered theoretically and experimentally in the year 1949 in Wagner

* Corresponding Author: Ismail Sakr

Email: ismailsakr@yahoo.com Telephone: +2-048-2333081

© 2013 All rights reserved. ISSR Journals

Fax: +2-048-2235695

PII: S2180-1363(13)5381-X

[2]. The influence of natural convection on the current distribution along the cathode and on the limiting current was investigated based on the boundary-layer theory [2]. The effect of migration on the limiting current in the presence of supporting electrolyte was studied in Selman and Newman [3]. Concentration and velocity profiles near vertical electrodes were investigated, e.g., in Awakura et al. [4] and Fukunaka et al. [5]. Local current density distributions along the cathode were studied, by Awakura et al. [6]. Recently, concentration profiles were measured experimentally by interferometry in Yang et al. [7].

In recent years, natural convection phenomena have also been investigated numerically. The influence of natural convection on the current density and the ionic concentration at the electrode was investigated by Kawai et al. [8] and [9]. Therein, the Laplace (electric potential field), the ion-transport (excluding migration effects), and the fluid equations were solved individually by a finite difference scheme. A galvanostatic boundary condition was introduced to keep the current flow at the electrodes constant over time. The numerical results were experimentally validated in Kawai et al. [10]. In Kawai et al. [11], the Butler-Volmer law was added as a kinetic boundary condition model. The importance of including density gradients for modeling rotating cylinder electrodes was emphasized in Mandin et al. [12]. The steady state ion-transport (excluding migration effects) and fluid equations were solved using a commercial software (CFX). Another finite difference scheme to simulate ion transfer (including migration effect) under the influence of natural convection was proposed in Volgin et al. [13]. In Chung [14], the tertiary current density distribution in the case of multi-ion electrodeposition was studied for high-aspect-ratio cells including convection, diffusion and migration. The flow, the ionic concentration and the potential field were strongly coupled by an iterative (two-dimensional) finite volume scheme. Natural convection phenomena were also investigated in Wallgren et al. [15] using a finite volume scheme, including an ion-transport equation for binary electrolyte solutions, an equation for the electric potential and the Butler-Volmer law as a kinetic boundary condition. Andreas et al. [16] has presented a novel computational approach for the numerical simulation of electrochemical systems influenced by natural convection phenomena. The computational framework was tested for various numerical examples exhibiting two- and three-dimensional electrochemical cell configurations including dilute CuSO_4 electrolyte solutions with and without excess of supporting H_2SO_4 electrolyte.

Gurniki et al. [17, 18] calculated turbulent mass transfer in nonlimiting current situations. They studied the use of large eddy simulations (LES) for predicting turbulent mass transfer in a parallel plate reactor, taking into account the turbulent fluctuations of the concentration. Only a binary electrolyte is considered which allowed the solution to be obtained in terms of one equivalent concentration $C = Z_1 C_1 = Z_2 C_2$. In order to model turbulent mass transfer, the turbulent fluid flow needs to be calculated. Nelissen et al. [19] solved the multi-ion transport and reaction model in turbulent flow. The model describes the effects of convection, diffusion, migration, chemical reactions and electrode reactions on the concentration, potential and current density distributions in an electrochemical reactor. The Reynolds averaged Navier–Stokes (RANS) equations were used to calculate the turbulent flow, with the turbulent viscosity obtained from a low-Reynolds number $k - \omega$ model. Different turbulence models for the turbulent mass transfer were examined and validated in a parallel plate reactor for the deposition of copper (Cu) from an acid copper-plating bath. The most accurate turbulent mass transfer models were the algebraic model for the turbulent diffusion and the newly suggested model with the constant turbulent Schmidt number equal to 4.5 by Nelissen et al. [19]. Experimental and numerical studies on the dynamics of flow and mass transfer in a tubular electrochemical reactor with cylindrical a mesh electrode were concerned by Ibrahim et al. [20]. The study was aimed for wastewater treatment. An improvement of the reactor only performance has been reached with higher flow rate.

The main objective of the present work is to develop a numerical code to simulate the turbulent flow through multi-ion transport and reaction model using finite volume method. The model describes the effects of convection, diffusion, migration, chemical reaction and electrode reaction on the concentration, potential and current density distribution in an electrochemical reactor. The Reynolds averaged Navier–Stokes (RANS) equations are used to calculate the turbulent flow case using the standard $k - \varepsilon$ (STD) model. In order to generate a decision on the quality of the code, the computational results are compared with available experimental data and with previous simulations.

2. Mathematical Model

2.1. Governing equations

In the present work, Multi-ion in a dilute electrolyte solution is considered for the time. The incompressible Navier-Stokes equations provide an adequate model to describe the flow of a multi-ion electrolyte solution in an electrochemical cell and the standard $k - \varepsilon$ (STD) model will be chosen to be an adequate turbulence model to represent the turbulence parameters.

The continuity equation:

$$\frac{\partial}{\partial x}(u) + \frac{\partial}{\partial y}(v) = 0.0 \quad (1)$$

x-momentum:

$$\rho \frac{\partial u}{\partial t} + \rho \left[u \frac{\partial u}{\partial x} + v \frac{\partial u}{\partial y} \right] = -\frac{\partial p}{\partial x} + \frac{\partial}{\partial x} \left[(\mu + \mu_t) \left(2 \frac{\partial u}{\partial x} \right) \right] + \frac{\partial}{\partial y} \left[(\mu + \mu_t) \left(\frac{\partial u}{\partial y} + \frac{\partial v}{\partial x} \right) \right] \quad (2)$$

y-momentum:

$$\begin{aligned} \dots \frac{\partial v}{\partial t} + \dots \left[u \frac{\partial v}{\partial x} + v \frac{\partial v}{\partial y} \right] = -\frac{\partial p}{\partial y} + \frac{\partial}{\partial x} \left[(\mu + \mu_t) \left(2 \frac{\partial v}{\partial y} \right) \right] + \frac{\partial}{\partial y} \left[(\mu + \mu_t) \left(\frac{\partial u}{\partial y} + \frac{\partial v}{\partial x} \right) \right] + \\ \dots g \sum_{i=1} S_i (C_i - C_{i,ref}) \end{aligned} \quad (3)$$

Turbulent kinetic energy:

$$\dots \frac{\partial k}{\partial t} + \dots \left[u \frac{\partial k}{\partial x} + v \frac{\partial k}{\partial y} \right] = \frac{\partial}{\partial x} \left[\left(\mu + \frac{\mu_t}{\Gamma_k} \right) \frac{\partial k}{\partial x} \right] + \frac{\partial}{\partial y} \left[\left(\mu + \frac{\mu_t}{\Gamma_k} \right) \frac{\partial k}{\partial y} \right] + P_k - \dots \nu \quad (4)$$

The rate of energy dissipation:

$$\dots \frac{\partial \nu}{\partial t} + \dots \left[u \frac{\partial \nu}{\partial x} + v \frac{\partial \nu}{\partial y} \right] = \frac{\partial}{\partial x} \left[\left(\mu + \frac{\mu_t}{\Gamma_\nu} \right) \frac{\partial \nu}{\partial x} \right] + \frac{\partial}{\partial y} \left[\left(\mu + \frac{\mu_t}{\Gamma_\nu} \right) \frac{\partial \nu}{\partial y} \right] + c_{v1} P_k \frac{\nu}{k} - \dots c_{v2} \frac{\nu^2}{k} \quad (5)$$

with the production term defined as:

$$P_k = \mu_t \left(2 \left(\frac{\partial u}{\partial x} \right)^2 + 2 \left(\frac{\partial v}{\partial y} \right)^2 + \left(\frac{\partial u}{\partial y} + \frac{\partial v}{\partial x} \right)^2 \right) \quad (6)$$

and the turbulent viscosity reads:

$$\mu_t = \dots C_\mu \frac{k^2}{\nu} \quad (7)$$

where u and v denote the mean velocities, ρ is the density, p is the pressure and μ is the laminar viscosity, k is the turbulent kinetic energy and ε is the dissipation energy.

2.2. Ionic species transport

The ionic - species mass flux in dilute solution Ni (mol/m².s) can be calculated using Planck–Nernst law expressed as in Newman and Thomas-Alyea [1]:

$$N_i = C_i v - (D_i + D_t) \nabla C_i - \frac{Z_i F D_i}{RT} C_i \nabla \phi \quad (8)$$

where C_i , D_i and Z_i are concentration (mol/m³), diffusivity (m²/s) and charge number of species i , respectively. ϕ represents the electric potential (volt), R is the universal gas constant (8.3143 J/mol.K), T denotes the temperature of the electrolyte solution (K) and F is the faraday constant (969485 C/mol),

while v is the velocity vector of the solvent (m/s). The first, second and third terms represent the convective, diffusive and migration contribution of mass flux, respectively. It is assumed that no homogeneous reactions take place in the solution, thus the equation for conservation of mass of species C_i becomes

$$\frac{\partial \dots C_i}{\partial t} = -\dots \nabla \cdot N_i \quad (9)$$

Hence from equations (8) the following equation can be obtained

$$\begin{aligned} \frac{\partial \dots C_i}{\partial t} + \dots u \frac{\partial C_i}{\partial x} + \dots v \frac{\partial C_i}{\partial x} = \frac{\partial}{\partial x} (\dots D_i + \frac{\tilde{t}_i}{\dagger_i}) \frac{\partial C_i}{\partial x} + \frac{\partial}{\partial y} (\dots D_i + \frac{\tilde{t}_i}{\dagger_i}) \frac{\partial C_i}{\partial y} \\ + \frac{\dots F Z_i D_i}{RT} \nabla \cdot (C_i \nabla \phi) \end{aligned} \quad (10)$$

The system of equations is typically closed by the so-called electroneutrality condition, in spite of the presence of charged species. This is true except for within very thin double layers adjacent to the electrodes whose effects are neglected in the present study:

$$\sum_i Z_i C_i = 0.0 \quad (11)$$

The current density due to the movement of an ionic species J (A/m^2) in the electrolyte is obtained by multiplying the ion flux by the corresponding charge number per mole in Newman and Thomas-Alyea [1]:

$$J = F \sum_i Z_i N_i \quad (12)$$

From equation (8), are can obtain the following equation

$$J = -\sum_i \frac{F^2 Z_i^2 D_i}{RT} C_i \nabla \phi - \sum_i F Z_i (D_i + D_t) \nabla C_i \quad (13)$$

To close the whole system, one more equation is needed to determine the potential field. It can be derived from the electric-current conservation,

$$\nabla \cdot J = 0.0 \quad (14)$$

This equation can be converted to potential ϕ equation is given by:

$$\nabla \cdot (|\nabla \phi|) + \nabla \cdot (\sum_i F Z_i (D_i + D_t) \nabla C_i) = 0.0 \quad (15)$$

where $|\nabla \phi| = \sum_i \frac{F^2 Z_i D_i C_i}{RT}$ is the electric conductivity.

2.2.1 Boundary condition:

The boundary conditions of multi-ion (Cu^{2+} , HSO_4 , and H^+) to be imposed are explained in Van den et al. [21] and Nelissen et al. [22].

At insulators and symmetry planes:

$$\frac{\partial W}{\partial n} = 0.0, \quad \frac{\partial C_i}{\partial n} = 0.0 \quad (16)$$

Where n is outward unit normal vector on the boundary of the computational domain.

At electrodes for non-reacting species (HSO_4 and H^+):

$$N_2 = 0.0, \quad N_3 = 0.0 \quad (17)$$

$$N_2 = -Z_2 D_2 \frac{F}{RT} C_2 \frac{\partial \phi}{\partial n} - (D_2 + D_t) \frac{\partial C_2}{\partial n} = 0.0 \quad (18)$$

$$N_3 = -Z_3 D_3 \frac{F}{RT} C_3 \frac{\partial \phi}{\partial n} - (D_3 + D_t) \frac{\partial C_3}{\partial n} = 0.0 \quad (19)$$

At electrodes for reacting species (Cu^{2+}):

$$N_1 = -Z_1 D_1 \frac{F}{RT} C_1 \frac{\partial \phi}{\partial x} - (D_1 + D_t) \frac{\partial C_1}{\partial n} = \frac{J}{Z_1 F} \quad (20)$$

From equations (18, 19 and 20) we obtain

$$\frac{\partial \phi}{\partial n} = \frac{-JRT}{F^2 (D_1 + D_t) \left[\frac{Z_1^2 D_1 C_{1ref}}{(D_1 + D_t)} + \frac{Z_2^2 D_2 C_{2ref}}{(D_2 + D_t)} + \frac{Z_3^2 D_3 C_{3ref}}{(D_3 + D_t)} \right]} \quad (21)$$

$$\frac{\partial C_1}{\partial n} = \frac{-J}{F Z_1 (D_1 + D_t)} + \frac{-JRT}{F^2 (D_1 + D_t) \left[\frac{Z_1^2 D_1 C_{1ref}}{(D_1 + D_t)} + \frac{Z_2^2 D_2 C_{2ref}}{(D_2 + D_t)} + \frac{Z_3^2 D_3 C_{3ref}}{(D_3 + D_t)} \right]} \quad (22)$$

$$\frac{\partial C_2}{\partial n} = \frac{J Z_2 D_2 C_{2ref}}{F (D_1 + D_t) (D_2 + D_t) \left[\frac{Z_1^2 D_1 C_{1ref}}{(D_1 + D_t)} + \frac{Z_2^2 D_2 C_{2ref}}{(D_2 + D_t)} + \frac{Z_3^2 D_3 C_{3ref}}{(D_3 + D_t)} \right]} \quad (23)$$

The normal current density J at the electrode is determined by an (often non-linear) kinetic model that typically depends on the solution variables. An important example is the Butler-Volmer law in the form Newman and Thomas-Alyea [1].

$$J = J_o \left(\frac{C_i}{C_{iref}} \right)^x \left[\exp\left(\frac{\alpha_a F}{RT} (V - \phi) \right) - \exp\left(\frac{\alpha_c F}{RT} (V - \phi) \right) \right] \quad (24)$$

The additional parameters involved are the exchange current density J_o , some reference concentration for the reactive ionic species C_{iref} , an exponent for weighting the surface concentration dependency, an anodic constant α_a , a cathodic constant α_c , and the potential V applied on the metal side of the electrode. The surface overpotential specified on the electrode surface is defined as $\eta = V - \phi$. In a macroscopic model, the surface overpotential is the driving force for an electrochemical reaction (see, e.g., J. Newman and Thomas-Alyea [1]). It describes the deflection from the equilibrium potential at which the net reaction rate is zero, since forward and backward reactions are in balance.

$$\text{at inlet: } C_i = C_{iref}, \quad \nabla \phi = 0.0 \quad (25)$$

$$\text{at outlet: } \nabla C_i = 0.0, \quad \nabla \phi = 0.0 \quad (26)$$

2.3. special case (two-species):

The special case of two species, corresponding to the dissociation of a single salt, is usually referred to as a binary electrolyte solution. In this particular case, the two ion-transport equations resulting from (10) can be expressed as a single convection-diffusion equation of the reacting ionic species $i = 1$: since

$$\frac{\partial \dots C}{\partial t} + \dots u \frac{\partial C}{\partial x} + \dots v \frac{\partial C}{\partial x} = \frac{\partial}{\partial x} \left(\dots D + \frac{\tilde{t}}{t} \right) \frac{\partial C}{\partial x} + \frac{\partial}{\partial y} \left(\dots D + \frac{\tilde{t}}{t} \right) \frac{\partial C}{\partial y} \quad (27)$$

with the diffusion coefficient D for this particular electrolyte solution given as (see, Newman and Thomas [1] and B.Georg et al. [23])

$$D = \frac{Z_1 D_1 D_2 - Z_2 D_2 D_1}{Z_1 D_1 - Z_2 D_2} \quad (28)$$

The concentration of the second ionic species $i = 2$ is related to the concentration C_1 by means of the electroneutrality condition see equation (11):

$$C_2 = -\frac{Z_1}{Z_2} C_1 \quad (29)$$

In equation (13), the current density J is eliminated

$$J = F \left[(Z_1 (D_2 + D_t) - Z_1 (D_1 + D_t)) \nabla C + \frac{Z_1 F}{RT} ((Z_2 D_2 - Z_1 D_1) C \nabla \phi) \right] \quad (30)$$

From equation (15), the potential ϕ is eliminated

$$\nabla^2 C + \frac{F}{RT} \left(\frac{Z_1 D_1 - Z_2 D_2}{(D_1 + D_t) - (D_2 + D_t)} \right) \nabla C \nabla \phi = 0.0 \quad (31)$$

The boundary conditions are concerned as the following:
at electrodes for reacting species:

$$N_1 = -Z_1 D_1 \frac{F}{RT} C_1 \frac{\partial \phi}{\partial n} - (D_1 + D_t) \frac{\partial C_1}{\partial n} = Z \frac{J}{Z_1 F} \quad (32)$$

at electrodes for non-reacting species:

$$N_2 = 0.0 \quad (33)$$

$$N_2 = -Z_2 D_2 \frac{F}{RT} C_2 \frac{\partial \phi}{\partial n} - (D_2 + D_t) \frac{\partial C_2}{\partial n} = 0.0 \quad (34)$$

Based on the condition of electroneutrality, we find from equations (17) and (19)

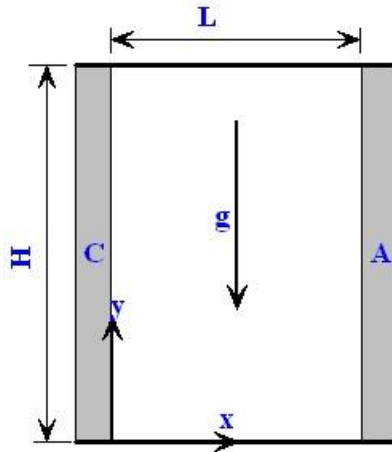
$$-D \frac{\partial C_1}{\partial n} = \frac{(1-t_1^*)}{Z_1 F} J \quad (35)$$

where $D = \frac{Z_1 D_1 (D_2 + D_t) - Z_2 D_2 (D_1 + D_t)}{Z_1 D_1 - Z_2 D_2}$ is called the binary electrolyte diffusion coefficient (for

laminar flow $D_t=0.0$) and $t_1^* = \frac{Z_1 D_1}{Z_1 D_1 - Z_2 D_2}$ is the transference number cation ion in a binary aqueous electrolyte solution in Newman and Thomas [1].

3. Numerical examples

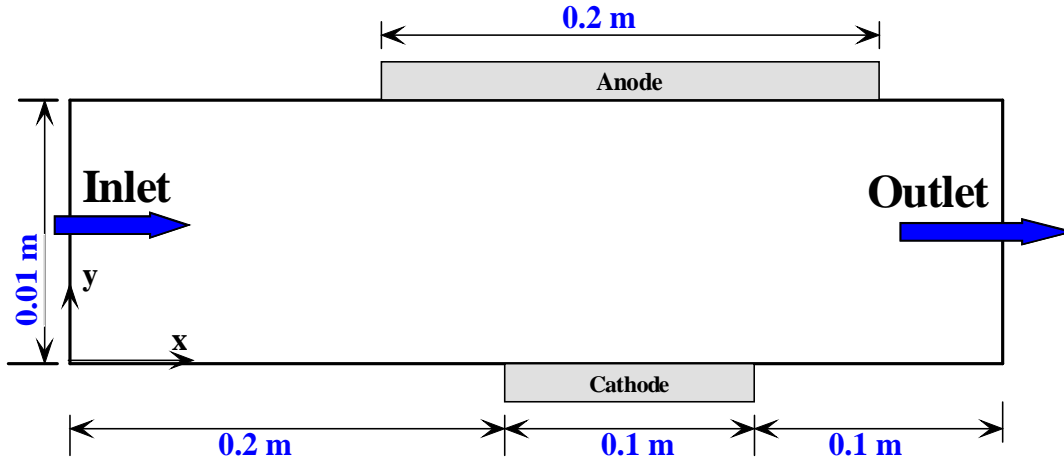
The computational domain and boundary conditions for natural convection between two vertical electrodes with supporting electrolyte are shown in Fig.1 (a) and considered to be Case 1. This case was previously experimentally and numerically considered by Kawai et al. [8]. A constant current density of 20 A/m² is applied to the Cu cathode immersed in a 0.6 M CuSO₄ aqueous electrolyte solution. The CuSO₄ aqueous electrolyte solution dissociates into Cu²⁺ and SO₄²⁻. The computational domain is discretized into 82x102 cells with uniform mesh and a constant time step $\Delta t = 1s$ is used for all simulations.



(a) Case 1: Electrochemical cell with vertical parallel electrode of Kawai et al. [8],
H[mm] = 10, L[mm] = 1 or 2. C: Cathode and A: Anode.

Fig.1 (Case 2) shows the geometry of two-dimensional parallel-plates electrochemical reactor electrodes in a multi-ion electrolyte solution including a copper deposition from 0.3 M CuSO₄ + 1 M H₂SO₄ electrolyte solution. Assuming complete dissociation as in [29], an ion-transport problem involving three ion species (Cu²⁺, HSO₄⁻, H⁺) is solved. The computational domain is discretized into 162x82 uniform mesh. The advantage of numerical examples shown in Fig.1 (b) boundary conditions including a Butler- Volmer

formulation is demonstrated for an electrolyte cell with parallel electrodes. The ionic properties of the solutions, containing two species and three species are given in Table 1. These data are taken from Kawai et al. [9]. Case 1 handles the unsteady natural cavity respectively while Case 2 is considered for steady turbulent flow.



(b)Case 2: Electrochemical reactor with parallel electrode of [19].

Figure 1. Representations of the computational domain for the considered cases:

(a) Case 1, and (b) Case 2.

TABLE 1: PHYSICAL PROPERTIES AND MODEL PARAMETERS

Case 1, unsteady , laminar (2 species)		Case 2, steady , turbulent (3 species)	
Electrolyte solution [9]	0.6 M CuSO ₄	Electrolyte solution [14,19]	0.3 M CuSO ₄ +1 M H ₂ SO ₄
C _{1ref} [mol/m ³]	600	C _{1ref} [mol/m ³]	300
C _{2ref} [mol/m ³]	600	C _{2ref} [mol/m ³]	1300
Z ₁ [-]	+2	C _{3ref} [mol/m ³]	700
Z ₂ [-]	-2	Z ₁ [-]	+2
D _{CuSO₄} [m ² /s]	4.42x10 ⁻¹⁰	Z ₂ [-]	-1
D _{Cu²⁺} [m ² /s]	7.12x10 ⁻¹⁰	Z ₃ [-]	+1
D _{SO₄²⁻} [m ² /s]	1.06x10 ⁻⁹	D ₁ [m ² /s]	0.61x10 ⁻⁹
t _{cu²⁺} [*] [-]	0.29	D ₂ [m ² /s]	1.065x10 ⁻⁹
ρ [kg/m ³]	1090	D ₃ [m ² /s]	9.312x10 ⁻⁹
μ [Pa.s]	1.31x10 ⁻³	ρ [kg/m ³]	1020
β [m ³ /mol]	1.4x10 ⁻⁴	μ [Pa.s]	1.105x10 ⁻³
T [K]	298	T [K]	298
Electrode Spacing L [mm]	1,2	Applied potential [volt]	0.6
Applied current densities J _{tot} [A/m ²]	20.0		
Properties required for Butler-Volmer BC [20]			
J ₀ [A/m ²]			25
γ [-]			0.75
α _a			0.5
α _c			0.25

4. Numerical method

The average transport equations for mass and momentum of flow as well as for the turbulence in flow can be written for unsteady, incompressible, two-dimensional flows in the following general transport equation form:

$$\frac{\partial \dots \{ \}}{\partial t} + \nabla \cdot (\dots u \{ \}) = -\nabla p + \nabla \cdot [\Gamma_{\{ \}} \nabla \{ \}] + S_{\{ \}} \quad (36)$$

TABLE 2: GOVERNING EQUATIONS OF ELECTROLYTE SOLUTION

Conservation of	$\{ \}$	$\Gamma_{\{ \}}$	$S_{\{ \}}$
Mass	1	0.0	0.0
Axial momentum	u	u_{eff}	$-\frac{\partial p}{\partial x} + \frac{\partial}{\partial x} \left(r \sim_{eff} \left(\frac{\partial u}{\partial x} \right) \right) + \frac{\partial}{\partial y} \left(r \sim_{eff} \frac{\partial v}{\partial x} \right)$
Radial momentum	v	u_{eff}	$-\frac{\partial p}{\partial r} + \frac{\partial}{\partial x} \left(\sim_{eff} \frac{\partial u}{\partial y} \right) + \frac{\partial}{\partial r} \left(\sim_{eff} \left(\frac{\partial v}{\partial y} \right) \right) + g S_{\dots} (C_i - C_{iref})$
Turbulent kinetic energy	k	$\frac{\sim_{eff}}{\dagger_k}$	$P - \dots v$
Dissipation rate	v	$\frac{\sim_{eff}}{\dagger_v}$	$\frac{v}{k} (C_{v1} P - C_{v2} \dots v)$
Species	C_i	$\dots D_i + \frac{\sim_t}{\dagger_i}$	$\frac{\dots F z_i D_i}{RT} \nabla \cdot (C_i \nabla \phi)$
Potential volt	ϕ		$\nabla \cdot \left(\sum_i F z_i (D_i + D_t) \nabla C_i \right)$

Where the variable $\{ \}$ is the dependent variable, representing the streamwise velocity u , the normal velocity v , the turbulence kinetic energy k , dissipation rate v , the ionic concentration C_i and potential volt ϕ , respectively. The diffusion coefficient $\Gamma_{\{ \}}$ and source term $S_{\{ \}}$ in the respective governing equation are specific to a particular meaning of ϕ , see Table 2.

The numerical method employed here to solve the above general differential equation is based on a general method for prediction of heat and mass transfer, fluid flow and related processes. This method has been developed and proved its generality and capability in a wide range of possible applications for predicting physically meaningful solutions even for uniform grid by Patanker, SV. [24]. The control volume integration of the above general differential equation yields a discretized form being solved numerically on a staggered grid system. The governing equations are discretized using the hybrid scheme to achieve the best accuracy. In the present work, the SIMPLE algorithm of parameter is employed. The algorithm is started with the solution of the discretized momentum equations according to the associated boundary and initial conditions.

5. Results

In order to evaluate the quality of the simulation, computations have been performed on different important test cases with two-dimensional forms. Natural convection between two vertical electrodes (Cavity form) with supporting electrolyte of constant current density is the first test case. The ability of the code to model turbulent mass transfer also, the turbulent flow in electrochemical reactor with parallel electrode (in a large duct) is also considered. Comparisons with the different available measurements and published numerical data corresponding to the mentioned cases will be presented in the following subsections.

5.1. Natural convection between two vertical electrodes in a binary electrolyte solution (Case 1: electrodes with constant current density)

Figs. 2 and 3 show the cation concentration profile and the stream function profile 700 s after the galvanostatic electrolysis starts. It is seen that the electrolyte is stratified at the top of cathode as well as the bottom of anode in Fig. 2.

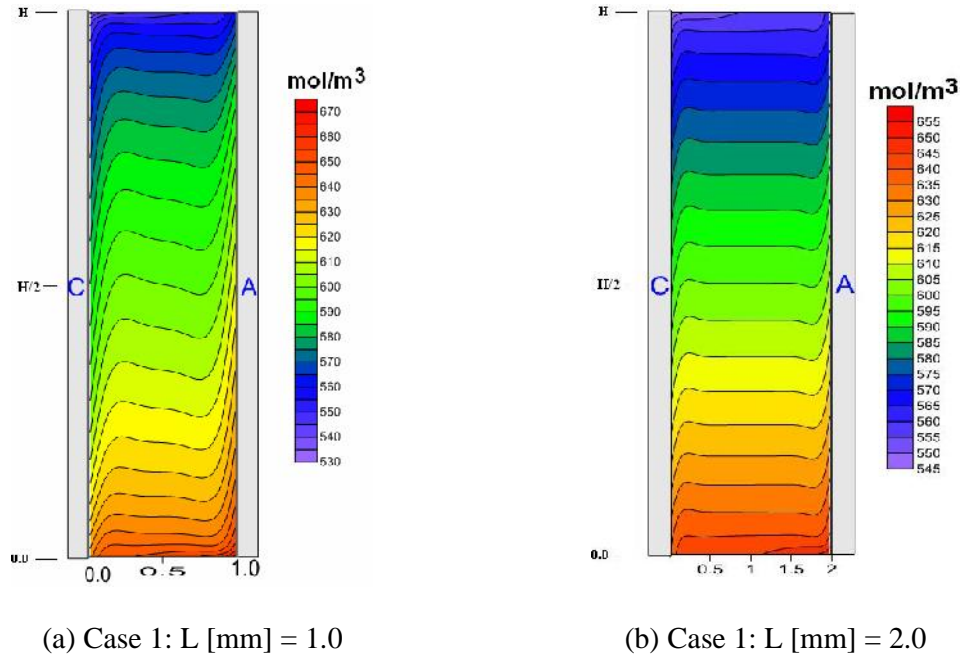
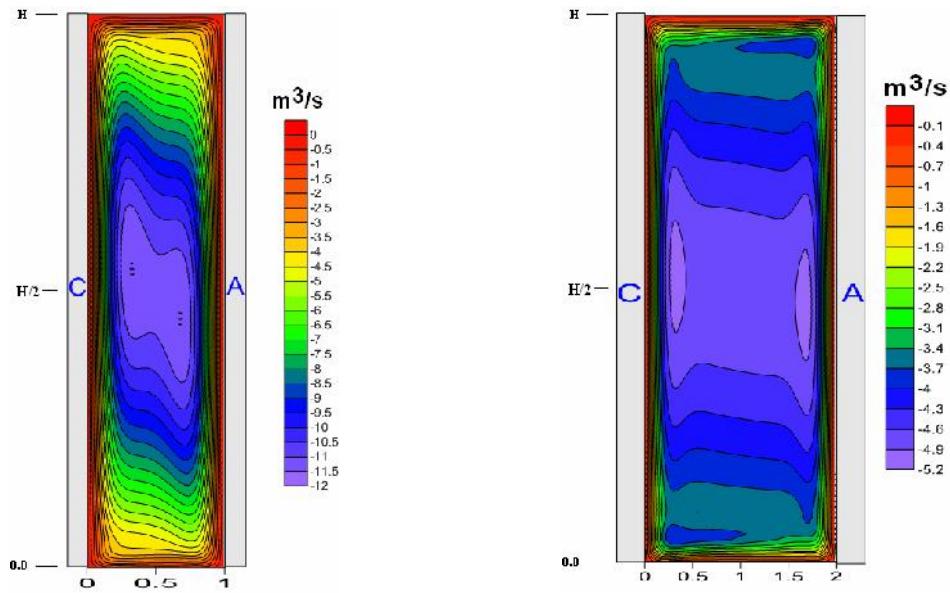


Figure 2 Concentration [mol/m³] profiles at 700 seconds after electrolysis starts in aqueous electrolyte solution containing 0.6 M CuSO₄, H[mm] = 10, J [A/m²] = 20.0.

From the stream function profile as demonstrated in Fig. 3, the clockwise fluid motion is seen in macroscopic scale. Both upper and lower end regions and an interior region can be distinguished. Moreover, difference due to the electrode space is found in the interior region of both flow patterns. The small and weak eddies are dissipated with time. The electrolyte solution near cathode becomes depleted of Cu²⁺ ion, so the electrolyte density becomes lower. Therefore, upward buoyancy acts to induce upward natural convection along a vertical plane cathode surface. At the same time, the electrolyte solution near anode becomes enriched with Cu²⁺ ion, so it becomes denser. Thus, downward natural convection is induced along a vertical plane anode. The clockwise fluid motion is then introduced in electrolyte as illustrated in Fig. 3. Bulk-electrolyte flows toward the cathode surface in the lower cathode and much lower concentration electrolyte flows toward bulk-electrolyte in the upper cathode. Near anode, vice versa occurs. Therefore, the electrolyte with lower concentration is accumulated near the top of cathode while that with higher concentration is stratified near the bottom of anode, respectively, as illustrated in Fig. 2.

To explicitly examine the validity of the code, the calculated fluid vertical velocity profile at mid-height of the cavity and the transient variation of electrode surface concentration are compared with the measurements and computations by Kawai et al. [8]. Figure 4 compares the calculated space variation of vertical component of fluid velocity v with the observed values by the tracer technique of Kawai et al. [8]. Maximum velocity is about 0.189(mm/s) at 0.156 (mm) from the cathode surface in the present simulation compared with 0.170 (mm/s) at 0.2 (mm) of the traced values of Kawai et al. [8]. From the cathode surface to this maximum value point, the calculated fluid velocity increases in a parabolic form. Then, it linearly decreases in the bulk-electrolyte to reach the anodic natural convection region. Figure 4 illustrates a quantitatively good agreement between the present observed and the calculated velocity profile of Kawai et al. [8] in the middle height of electrode.



(a) Case 1: L [mm] = 1.0

(b) Case 1: L [mm] = 2.0

Figure 3 Stream function (m^3/s) profiles at 700 seconds after electrolysis starts in aqueous electrolyte solution containing 0.6 M CuSO_4 , $H[\text{mm}] = 10$, $J [\text{A}/\text{m}^2] = 20.0$.

Fig. 5 reasonably compares the calculated transient variation at the mid-height point of both cathode and anode surface concentration with the measurements and computations of Kawai et al. [8].

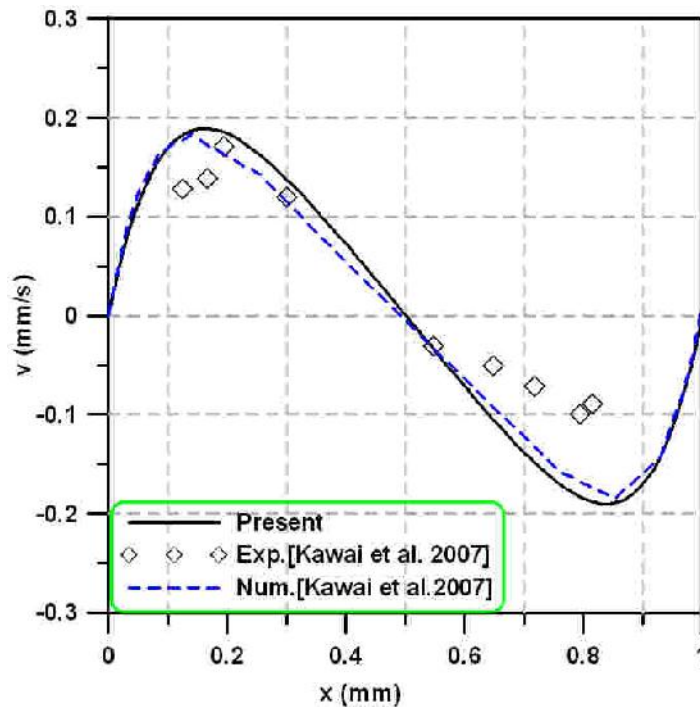


Figure 4 Case 1: Space variation of vertical component of fluid velocity at mid-height in aqueous electrolyte solution containing 0.6M CuSO_4 . $L [\text{mm}] = 1.0$, $J [\text{A}/\text{m}^2] = 20.0$, $t[\text{s}] = 50$. Comparisons with measurements and computations of [8].

The concentration linearly varies with the square root of time over initial 36 s. This is clearly observed in the present computation as well as that of Kawai et al. [9]. It must be primarily governed by the transient

diffusive ionic mass transfer rate. Then, the convective ionic mass transfer phenomenon starts to prevail to reach substantially constant concentration, then it experiences the overshooting phenomenon where an extreme value is recorded around 50–100 s.

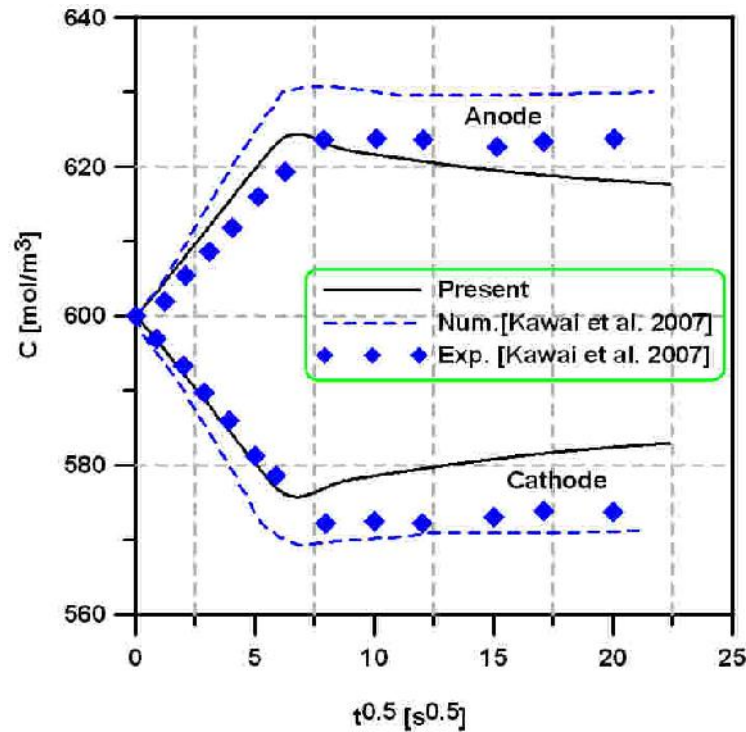


Figure 5 Case 1: Transient variation of electrode surface concentration at mid-height in aqueous electrolyte solution containing 0.6M CuSO_4 . Cathode and Anode surface concentration. L [mm] = 1.0, J [A/m^2] = 20.0. Comparisons with measurements and computations of [8].

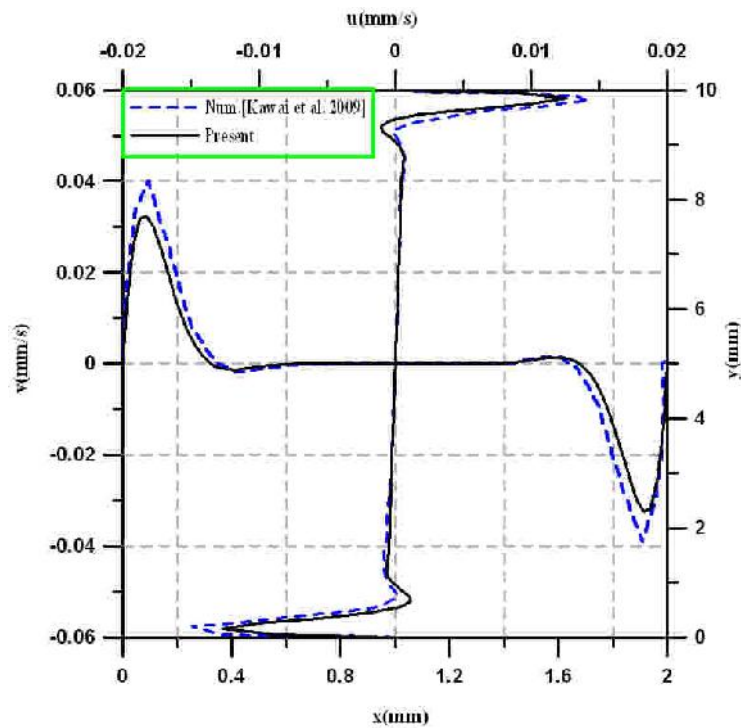


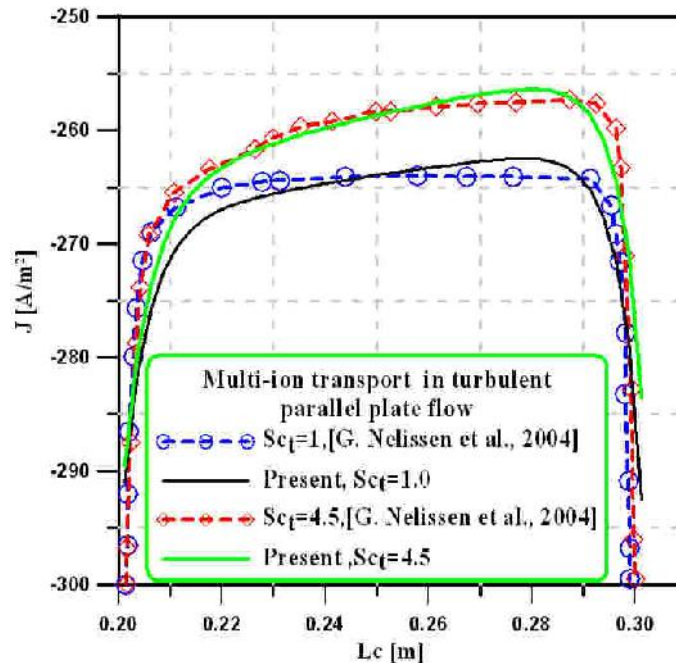
Figure 6 Case 1: Velocity profile at the steady state, $u(y)$ along line x [mm] = 1, $v(x)$ along line y [mm] = 5, t [s] = 6000. Comparison with simulation of [9].

However, the present simulations agree well the measurement of Kawai et al. [8]. Near both cathode and anode convective flow developing independently of each other are observed, while no detectable flow can be observed in an interior region and the collision process of both convective roles is not clearly observed. It may be partly due to the very narrow electrode spacing. However, the overshooting phenomena in both concentration and velocity profiles are clearly demonstrated. This phenomenon introduces the less significant contribution due to convective ionic mass transfer rate. The small eddies are dissipated by viscous stress particularly around $Re = 1$ as shown in Fig. 3. The cause of overshooting phenomenon depends on both the electrode spacing and applied current density. In order to capture the flow characteristics, Fig. 6 is plotted showing the horizontal component of the fluid velocity on line x [mm] = 1 and the vertical component on line y [mm] = 5 at t [s] = 6000, while a reasonable agreement with numerical results of Kawai et al. [9] is noticed.

5.2 Turbulent flow between parallel electrodes in a multi-ion electrolyte solution (Case 2: electrodes with Butler-Volmer equation of current density)

In this case, the turbulent flow in a parallel electrode in a multi-ion solution (See Fig. 1.b) is calculated and validated with literature results. The reference results are numerically obtained from the low - Reynolds $k - \tilde{\sigma}$ model of Nelissen et al. [19] because of the absence of experimental data for such case. The Reynolds number, based on the average inlet velocity and the height of the cell is $Re=8333$ and the turbulent Schmidt number, equivalent to the turbulent Prandtl number in heat transfer, is defined as: $Sc_t = \frac{\epsilon_t}{D_t}$. In the present work the standard $k - \nu$ model is used to calculate the flow

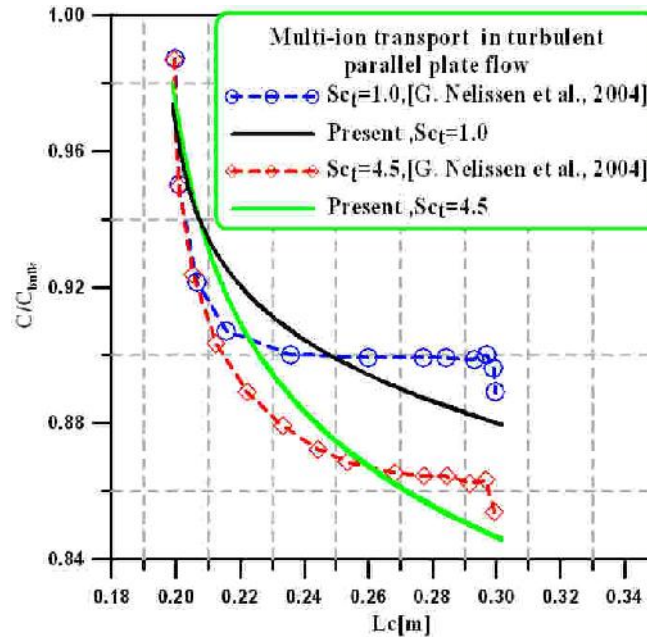
turbulence in a parallel plate reactor with different turbulent Schmidt number ($Sc_t=1$ and 4.5). The electrolyte consists of 0.3 M $CuSO_4+1$ M H_2SO_4 , which is quite within the industrial concentration range of acid copper-plating baths. The ionic properties of this electrolyte, containing three species (Cu^{2+} , HSO_4 and H^+) are shown in Table 2, obtained from Chung [14].



(a) Current-density distributions

In what follows, calculations using the multi-ion transport and reaction model are performed using the different turbulent Schmidt number mentioned above. The aim is to study the ability of standard $k - \epsilon$ to compute the current density and concentration profiles in such complex case. Calculations with a constant imposed potential difference between anode and cathode equal to 600 [mV] are performed.

Both anode and cathode are supposed to have a constant metal potential, due to their high electrical conductivity. The resulting concentration and current density profiles for two different turbulence Schmidt number are shown in Fig. 7.



(b) Concentration distributions

Figure 7 Case 2: Distributions of current density (a) and concentration of the Cu^{2+} ion (b) along the cathode for an imposed potential difference of 600 [mVolt], $Re = 8333$, $Sc_t=1$ and 4.5. Comparisons with [19].

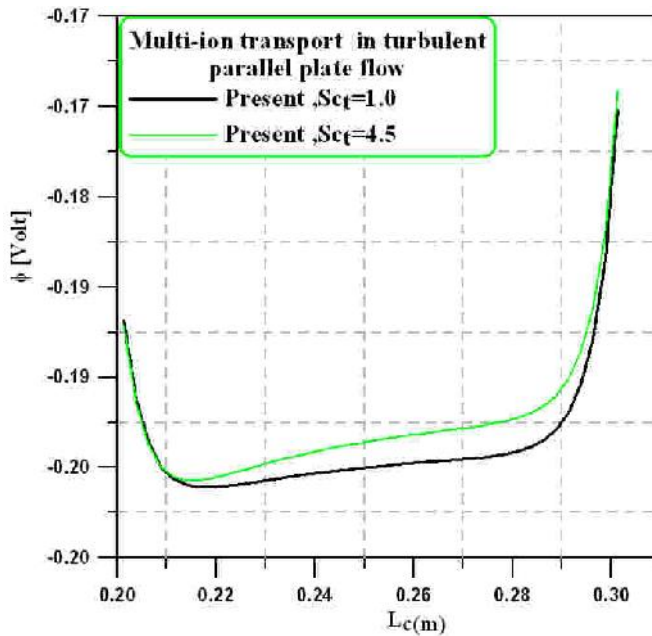


Figure 8 Case 2: Cathode potential at different Sc_t and $Re = 8333$.

It is clear that the variation in the turbulent diffusion coefficients according to the turbulence Schmidt number leads to differing current density as well as concentration distributions. The model $Sc_t=4.5$ that overestimates the turbulent diffusion, results in the highest current density and the smallest

concentration. To this moment there are no experimental results to draw decisive conclusions on the influence of turbulent mass transfer on the multi-ion transport and reaction model. The numerical results show a reasonable agreement with the computations of [19].

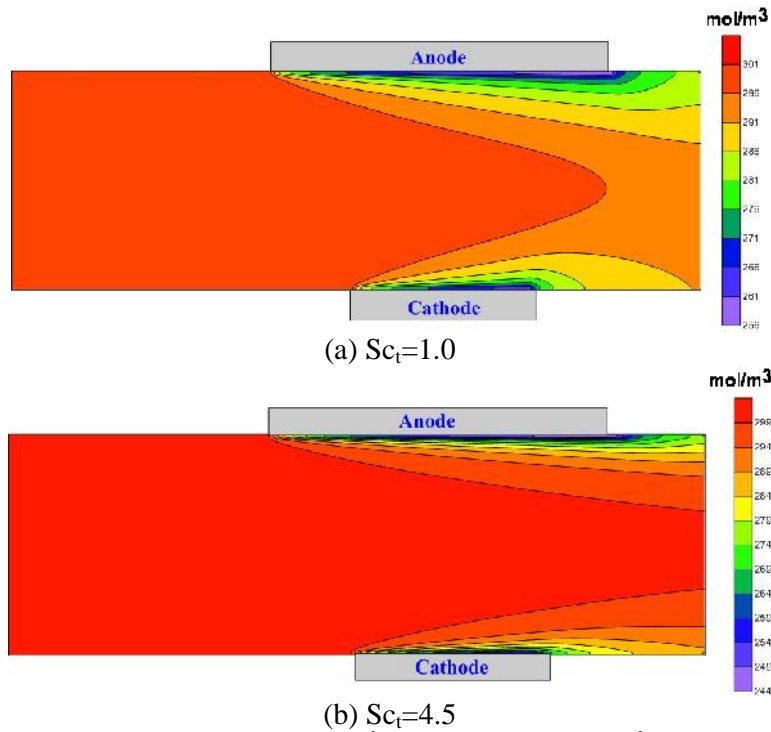


Figure 9 Case 2: Concentration (mol/m^3) contour of the Cu^{2+} ion for an imposed potential difference of 600 [mVolt], $\text{Re} = 8333$, (a) $\text{Sc}_t=1.0$ and (b) $\text{Sc}_t=4.5$.

However, the small deviation in the concentration distributions refers to the used turbulence model. Figure 8 shows the potential at different turbulence Schmidt numbers on the cathode surface.

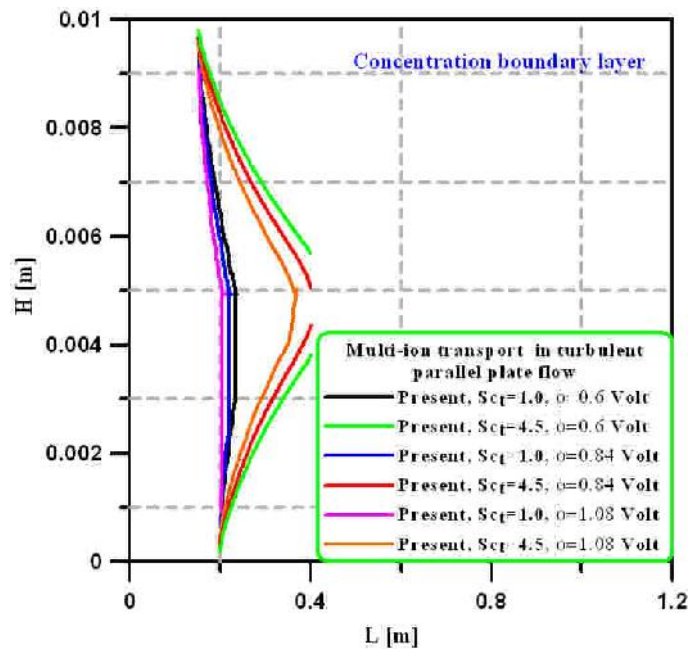


Figure 10 Case 2: Mass concentration boundary layer at different potential difference, $\text{Re}=8333$, $\text{Sc}_t=1$ and 4.5.

The increase of the volt with the turbulent Schmidt number can be explained as the decrease of concentration. Figure 9 shows the concentration contours at different Schmidt numbers. It is observed from Fig. 9 that the contours are smooth and show different concentration boundary layers along the electrodes at different turbulent Schmidt number. It is observed that the thickness of concentration boundary layer decreases with the increase of turbulent Schmidt number at the same potential volt 600 [mVolt]. Fig. 10 shows the mass concentration boundary layer thickness H (m) at different overpotential volt and different turbulent Schmidt number. It is observed from Fig. 10 that the thickness of concentration boundary layer increases with the increase of overpotential volt at the same turbulent Schmidt number. However, with the increase turbulent Schmidt number the concentration boundary layer thickness decreases.

6. Conclusions

A numerical study has been performed to simulate the natural and forced flows in a chemical solution. In the case of turbulent flow, the standard $k - \nu$ model has been chosen to simulate the turbulence behaviors. Different test cases have been introduced to check the ability and the quality of the developed code. The test cases include the flow and mass transfer between vertical and horizontal plates filled with cathode and anode. The results include the concentration, potential, current density and the development of concentration boundary layer under different Schmidt numbers. Comparisons with the available experimental measurements as well as previous numerical data showed the ability of the present developed code in capturing the complex behaviors of flow and mass transfer in such different cases.

References

- [1] J. Newman, K. E. Thomas-Alyea, *Electrochemical Systems* (3rd ed.), John Wiley & Sons, Inc., Hoboken; New Jersey, (2004).
- [2] C. Wagner, The role of natural convection in electrolytic processes, *J. Electrochem. Soc.* 95 (1949) 161–173.
- [3] J. R. Selman, J. Newman, Free-convection mass transfer with a supporting electrolyte, *J. Electrochem. Soc.* 118 (1971)1070–1078.
- [4] Y. Awakura, Y. Takenaka, Y. Kondo, Studies on the velocity profile in natural convection during copper deposition at vertical cathodes, *Electrochim. Acta* 21 (1976) 789 – 797.
- [5] Y. Fukunaka, K. Denpo, M. Iwata, K. Maruoka, Y. Kondo, Concentration profile of Cu^{2+} ion near a plane vertical cathode in electrolytes containing CuSO_4 and an excess of H_2SO_4 as a supporting electrolyte, *J. Electrochem. Soc.* 130(1983) 2492–2499.
- [6] Y. Awakura, E. Ebata, Y. Kondo, Distribution of local current densities during copper electrodeposition on a plane vertical cathode, *J. Electrochem. Soc.* 126 (1979) 23–30.
- [7] X. Yang, K. Eckert, A. Heinze, M. Uhlemann, The concentration field during transient natural convection between vertical electrodes in a small-aspect-ratio cell, *J. Electroanal.Chem.* 613 (2008) 97–107.
- [8] S. Kawai, Y. Fukunaka, S. Kida, Numerical simulation of transient natural convection induced by electrochemical reactions confined between vertical plane Cu electrodes, *Electrochimica Acta* 53 (2007) 257–264
- [9] S. Kawai, Y. Fukunaka, S. Kida, Numerical simulation of ionic mass-transfer rates with natural convection in CuSO_4 - H_2SO_4 solution, I. Numerical study on the developments of secondary flow and electrolyte stratification phenomena, *J. Electrochem. Soc.* 156 (2009) 99–108
- [10] S. Kawai, Y. Fukunaka, S. Kida, Numerical simulation of ionic mass-transfer rates with natural convection in CuSO_4 - H_2SO_4 solution, II. Comparisons between numerical calculations and optical measurements, *J. Electrochem. Soc.* 156 (2009) 109–114.
- [11] S. Kawai, Y. Fukunaka, S. Kida, Numerical calculation of transient current density distribution along vertical plane electrode in CuSO_4 - H_2SO_4 electrolyte solution, *J. Electrochem. Soc.* 157 (2010) 40–48.

- [12] P. Mandin, J. M. Cense, B. Georges, V. Favre, T. Pauport'e, Y. Fukunaka, D. Lincot, Prediction of the electrode position process behavior with the gravity or acceleration value at continuous and discrete scale, *Electrochim. Acta* 53 (2007)233–244.
- [13] V. M. Volgin, O. V. Volgina, D. A. Bograchev, A. D. Davydov, Simulation of ion transfer under conditions of natural convection by the finite difference method, *J. Electroanal. Chem.* 546 (2003) 15–22.
- [14] M. H. Chung, A numerical method for analysis of tertiary current distribution in unsteady natural convection multi-ion electrodeposition, *Electrochim. Acta* 45 (2000) 3959–3972
- [15] C. F. Wallgren, F. H. Bark, R. Eriksson, D. S. Simonsson, J. Persson, R. I. Karlsson, Mass transport in a weakly stratified electrochemical cell, *J. Appl. Electrochem.* 26 (1996) 1235–1244.
- [16] A. Ehrl, G. Bauer, V. Gravemeier, W.A. Wall, A computational approach for the simulation of natural convection in electrochemical cells, *Journal of Computational Physics* 235 (2013) 764–785
- [17] F. Gurniki, K. Fukagata, S. Zahrai, F.H. Bark, Turbulent free convection in large electrochemical cells with a binary electrolyte, *J. Appl.Electrochem.* 29 (1999) 27.
- [18] F.Gurniki, S.Zahrai, F.H.Bark, LES of turbulent channel flow of a binary electrolyte, *J. Appl.Electrochem.* 30 (2000) 1335.
- [19] G. Nelissen, A. VanTheemsche ,C. Dan, B. Van den Bossche, J. Deconinck, Multi-ion transport and reaction simulations in turbulent parallel plate flow, *Journal of Electroanalytical Chemistry* 563 (2004) 213–220
- [20] D. S. Ibrahim, C. Veerabahu, R. Palani, S. Devi, N. Balasubramanian, Flow dynamics and mass transfer studies in a tubular electrochemical reactor with a mesh Electrode, *Computers & Fluids* 73 (2013) 97–103.
- [21] G. Nelissen, A. VanTheemsche ,C. Dan, B. Van den Bossche, J. Deconinck, Multi-ion transport and reaction simulations in turbulent parallel plate flow, *Journal of Electroanalytical Chemistry* 563 (2004) 213–220
- [22] G. Nelissen, B. Van den Bossche, J. Deconinck, A. VanTheemsche, C. Dan, Laminar and turbulent mass transfer simulations in a parallel plate reacto, *J. Appl.Electrochem.* 33 (2003) 863.
- [23] G. Bauer, V. Gravemeier, W.A. Wall, A 3D finite element approach for the coupled numerical Simulation of electrochemical systems and fluid flow, *I.J.for numerical methods in engineering*, 86 (2011) 1339–1359.
- [24] Patankar, S.V. (1980): Numerical heat transfer and fluid flow. Hemisphere Pub.Washington, DC, 1980.